

Elliptical polarization in VCSELs via joint interaction of a tilted sub-wavelength grating and intrinsic semiconductor anisotropies

Original

Elliptical polarization in VCSELs via joint interaction of a tilted sub-wavelength grating and intrinsic semiconductor anisotropies / Torrelli, Valerio; Miri, Lorenzo; D'Alessandro, Martino; Gullino, Alberto; Zimmer, Michael; Dahler, Katharina; Jetter, Michael; Michler, Peter; Elsässer, Wolfgang; Bertazzi, Francesco; Tibaldi, Alberto; Debernardi, Pierluigi. - In: OPTICS LETTERS. - ISSN 0146-9592. - STAMPA. - 50:9(2025), pp. 3082-3085. [10.1364/ol.557703]

Availability:

This version is available at: 11583/2999853 since: 2025-05-12T06:35:05Z

Publisher:

Optica Publishing Group

Published

DOI:10.1364/ol.557703

Terms of use:

This article is made available under terms and conditions as specified in the corresponding bibliographic description in the repository

Publisher copyright

Optica Publishing Group (formely OSA) postprint/Author's Accepted Manuscript

“© 2025 Optica Publishing Group. One print or electronic copy may be made for personal use only. Systematic reproduction and distribution, duplication of any material in this paper for a fee or for commercial purposes, or modifications of the content of this paper are prohibited.”

(Article begins on next page)

Elliptical polarization in VCSELs via joint interaction of a tilted subwavelength grating and intrinsic semiconductor anisotropies

VALERIO TORRELLI^{1,2}, LORENZO MIRI^{1,*}, MARTINO D'ALESSANDRO^{1,2}, ALBERTO GULLINO², MICHAEL ZIMMER³, KATHARINA DAHLER³, MICHAEL JETTER³, PETER MICHLER³, WOLFGANG ELSÄSSER^{2,4,5}, FRANCESCO BERTAZZI¹, ALBERTO TIBALDI¹, AND PIERLUIGI DEBERNARDI²

¹Department of Electronics and Telecommunications (DET), Politecnico di Torino, Corso Duca degli Abruzzi, 24, 10129 Torino, Italy

²Istituto di Elettronica e di Ingegneria dell'Informazione e delle Telecomunicazioni (IEIIT) del Consiglio Nazionale delle Ricerche (CNR), Politecnico di Torino, Italy

³Institut für Halbleiteroptik und Funktionelle Grenzflächen, Center for Integrated Quantum Science and Technology (IQST) and Research Center SCoPE, Universität Stuttgart, Allmandring 3, 70569 Stuttgart, Germany

⁴Institute of Applied Physics, Technische Universität Darmstadt, Schlossgartenstrasse 7 Darmstadt 64289, Germany

⁵School of Physics, Trinity College Dublin, Dublin 2, Ireland

*lorenzo.miri@polito.it

Compiled May 12, 2025

We demonstrate numerically and experimentally that, in vertical-cavity surface-emitting lasers (VCSELs), an originally non-chiral cavity can be converted into a chiral cavity by the interaction between a sub-wavelength grating tilted with respect to the crystalline axes and the intrinsic semiconductor optical anisotropies, *i.e.*, electro- and elasto-optic effects, thus enabling the emission of elliptically polarized light. The measured Stokes parameters of such a VCSEL, realized by a standard grating based VCSEL fabrication process, are fully in-line with the modeling results and confirm that, in dependence on the grating parameters, the full Poincaré sphere including circularly polarized can be covered on-demand.

<http://dx.doi.org/10.1364/ao.XX.XXXXXX>

Introduction. In recent years, vertical-cavity surface-emitting lasers (VCSELs) have become the predominant coherent light sources for a variety of established applications, such as short-haul optical interconnects [1, 2] and 3D sensing [3]. However, even though VCSELs were originally appealing for their reduced power consumption, a demand for high-power single-mode VCSELs arose from novel applications such as LiDAR and devices based on optical atomic pumping [4]. The latter represents a class of devices including quantum gyroscopes [5, 6], atomic clocks [7] and atomic magnetometers [8], relying on more compact light sources such as VCSELs to scale down their size to the chip scale [9]. Typical requirements for the laser source are high-power single transverse mode with a stable linear polarization in output [10, 11]. State-of-the-art VCSELs are currently able to emit a stable linear polarization due to the introduction of gratings [12–15], making them a suitable candidate for such new applications. However, atomic devices also require

circularly polarized (CP) light, needed to excite the required atomic transitions [9]. This is currently achieved by the usage of a quarter-wave plate to convert the VCSEL output polarization from linear to circular. This limits the scale-down of atomic devices, raising the need for native CP emitters. In the VCSEL field, various possibilities to achieve such a result are investigated in [16], focusing on 3D cavity chirality via the introduction of misaligned optical anisotropies.

In this work, we aim to harness the capabilities of sub-wavelength grating (SWG) VCSELs to inherently emit custom polarization states by tilting the grating bars with respect to the crystalline axis of the device. Building on the model outlined in [16], we investigated the combined effect of intrinsic anisotropies, such as electro- and elasto-optic effects, aligned with the crystalline axes, together with the extrinsic anisotropy introduced by the tilted SWG. The validation of our model through comparison with experimental data opens new possibilities for polarization engineering in standard grating VCSELs, enabling on-demand access to any desired polarization state.

Structure under investigation. The considered AlGaAs-VCSEL, emitting at $\lambda = 850$ nm, is grown epitaxially by metal-organic vapor-phase epitaxy (MOVPE) on an n-doped GaAs substrate with a donor concentration of $N_D = 2 \times 10^{18} \text{ cm}^{-3}$. The bottom n-doped ($N_D = 1.5 \times 10^{18} \text{ cm}^{-3}$) distributed Bragg reflector (DBR) comprises 30 pairs of $\text{Al}_{0.10}\text{Ga}_{0.90}\text{As}/\text{Si}$ / $\text{Al}_{0.95}\text{Ga}_{0.05}\text{As}/\text{Si}$ layers. Each layer has a thickness of $\lambda / (4n_r)$, where n_r is its refractive index. Above the bottom DBR, an intrinsic λ -cavity made of $\text{Al}_{0.50}\text{Ga}_{0.50}\text{As}$ embeds the active region (AR), which provides optical gain to support lasing. The top p-doped ($N_A = 1.5 \times 10^{18} \text{ cm}^{-3}$) DBR consists of 19.5 pairs of $\text{Al}_{0.20}\text{Ga}_{0.80}\text{As}/\text{Zn}$ / $\text{Al}_{0.95}\text{Ga}_{0.05}\text{As}/\text{Zn}$, connected by a linear molar fraction grading of 26 nm. Following the cavity, a high aluminum content layer ($\text{Al}_{0.98}\text{Ga}_{0.02}\text{As}$) is introduced for oxidation, allowing the transverse definition of

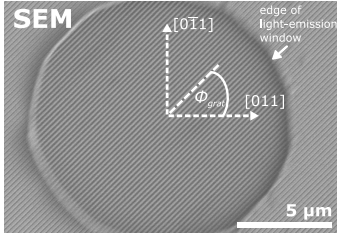


Fig. 1. Scanning electron microscope (SEM) picture of the light-emission window of a VCSEL. The SWG is tilted by the angle ϕ_{grat} .

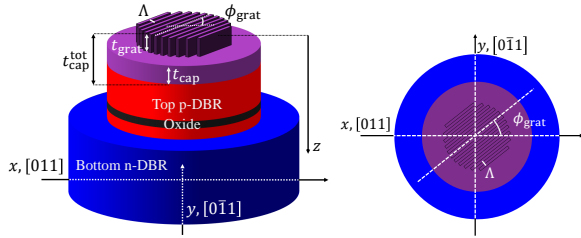


Fig. 2. Sketch of the investigated VCSEL structure, together with the reference system and the definition of the most relevant dimensions.

the oxide aperture, which confines both carriers and light.

The out-of-phase top DBR is turned in-phase by a heavily p-doped GaAs cap layer with an acceptor concentration of $N_A = 1 \times 10^{19} \text{ cm}^{-3}$ and a total thickness of $t_{\text{cap}}^{\text{tot}} = 3\lambda / (4n_r) = 175 \text{ nm}$, which also serves as contact layer.

To enable polarization control, a SWG is defined in a first processing step by electron-beam lithography and subsequently etched into the cap layer with a spatial period $\Lambda = 200 \text{ nm}$ by inductively-coupled plasma (ICP)-etching. The grating extends to a depth of $t_{\text{grat}} = \lambda / (2n_r) = 116 \text{ nm}$, leaving a residual cap layer thickness of $t_{\text{cap}} = t_{\text{cap}}^{\text{tot}} - t_{\text{grat}} = 59 \text{ nm}$. In Fig. 1, we show a SEM image of the resulting SWG.

The reference coordinate system is aligned to the crystal directions ($x = [011]$, $y = [0\bar{1}1]$), and the longitudinal z -axis opposite to the growth direction. The subsequent device fabrication follows a standard VCSEL process. Mesas are defined by a combination of photolithography and ICP-etching. The current confining oxide aperture is formed by wet-thermal oxidation of the $\text{Al}_{0.98}\text{GaAs}:\text{Zn}$ layer in an oxidation oven. Thereon, a $4 \mu\text{m}$ BCB isolation layer is spun on the sample and structured via UV-lithography. In the last processing steps the p-contact is defined by photolithography and deposited by electron beam evaporation, before evaporation of the n-contact completes the fabrication process.

To investigate the effect of the tilting angle ϕ_{grat} (displayed in Fig. 2) between the crystal axes and the grating bars, many identical samples with different ϕ_{grat} values ranging from 0° to 180° in steps of 5° are manufactured and analyzed, both experimentally and through simulations. This comprehensive approach ensures that the polarization features are thoroughly understood in all conditions. As the device operates in a single transverse mode, a one-dimensional electro-optical simulation along the z -axis is sufficient to capture its polarization characteristics. Fig. 2 shows a schematic of the structure.

Simulation methodologies. Our SWG VCSEL supports two

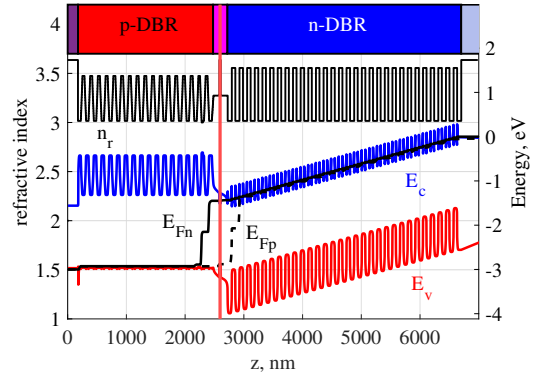


Fig. 3. Band diagram of the VCSEL together with the refractive index profile. The refractive index curve is read on the left axis, while all energies are read on the right axis. The vertical red line highlights the active region.

modes with identical spatial intensity distribution, but different polarizations, with different threshold gains and emission wavelengths. The mode with the lowest threshold is referred to as lasing polarization. To investigate this problem, a 1D vectorial optical simulation can be performed along the z axis. Our in-house vectorial 1D VCSEL ELectroMagnetic Suite (VELMS) [16] serves as optical mode solver. From the anisotropic refractive index longitudinal profile, one obtains the modal features of the two polarizations in terms of emission wavelengths, threshold gains, standing wave (SW) profiles, *i.e.*, modulus square of the optical field, and the electric field phasors, *i.e.*, Jones vectors, at the outcoupling facet of the laser. The Jones vector for the lasing polarization can be written as $\mathcal{E} = \mathcal{E}_x \mathbf{x} + \mathcal{E}_y \mathbf{y}$, $\mathcal{E}_x, \mathcal{E}_y \in \mathbb{C}$. The corresponding Stokes parameters [17, 18] are defined as

$$S_0 = |\mathcal{E}_x|^2 + |\mathcal{E}_y|^2, \quad (1a)$$

$$S_1 = \frac{|\mathcal{E}_x|^2 - |\mathcal{E}_y|^2}{S_0} \in [-1, +1], \quad (1b)$$

$$S_2 = \frac{+2\Re\{\mathcal{E}_y^* \mathcal{E}_x\}}{S_0} \in [-1, +1], \quad (1c)$$

$$S_3 = \frac{-2\Im\{\mathcal{E}_y^* \mathcal{E}_x\}}{S_0} \in [-1, +1], \quad (1d)$$

The lasing polarization results from the competition of optical anisotropies, creating a chiral resonator when they are misaligned [16]. In the structure of Fig. 2 two anisotropies are present: the tilted SWG and the electro-optic effect (EOE). VELMS propagates the field in the resonator using the transmission matrices of the layers and imposing the cavity roundtrip Barkhausen criterion. The transmission matrix of the SWG is computed by rigorous coupled wave analysis [19, 20]. On the other hand, the anisotropy arising from the EOE can be evaluated in terms of the semi-difference of the relative dielectric constants along x , $\epsilon_{xx} = n_{xx}^2$, and y , $\epsilon_{yy} = n_{yy}^2$, as [21]

$$\Delta\epsilon_{\text{EOE}}(z) = \frac{\epsilon_{xx} - \epsilon_{yy}}{2} = n_r^4(z) r_{41}(z) E(z), \quad (2)$$

where $n_r(z)$ is the refractive index profile in the absence of the optical anisotropies induced by the electro-optic and elastooptic effects, $E(z)$ is the z -component of the electrostatic field

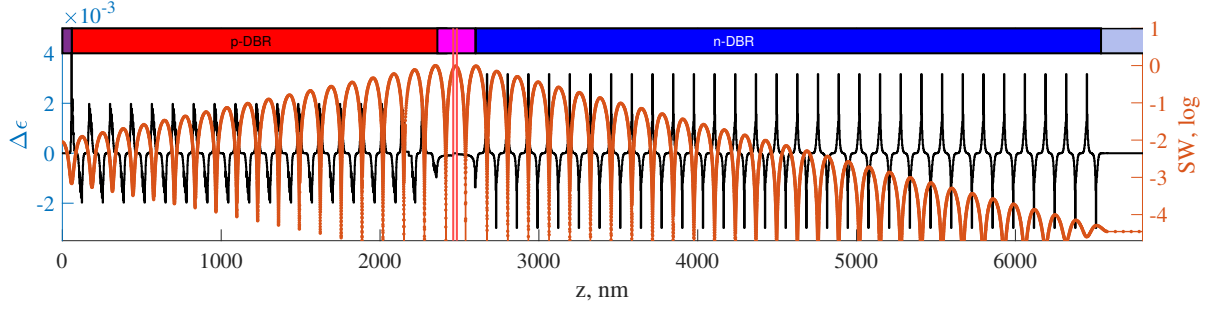


Fig. 4. SW and anisotropy profile resulting from the EOE, showing that only negative peaks of $\Delta\epsilon$ are relevant to the optical mode.

118 profile and $r_{41} = 1.6$ pm/V for GaAs [22], and 0.78 pm/V
 119 for AlAs [23]. Intermediate aluminum molar fractions are linearly
 120 interpolated. $E(z)$ is obtained with our in-house 1D drift-
 121 diffusion (DD) code [24, 25] and is mainly governed by the
 122 doped heterostructures of the DBRs. Finally, if a uniform strain σ
 123 (adimensional) is mechanically applied along the crystal axes
 124 an additional anisotropy results as consequence of the elasto-
 125 optic effect. The equivalent of Eq. (2) for the elasto-optic effect
 126 reads

$$\Delta\epsilon_{\sigma} = n_r^4(z) p_{44} \frac{\sigma}{2}, \quad (3)$$

127 where $p_{44} = 0.072$ [21]. The overall anisotropy $\Delta\epsilon = \Delta\epsilon_{\text{EOE}} +$
 128 $\Delta\epsilon_{\sigma}$ can be evaluated as the sum of the two effects.

129 **Experimental characterization.** The VCSEL characterization
 130 setup features a temperature-cooled copper plate that also serves
 131 as the n-electrode on which the device under investigation is
 132 placed. The p-side of the VCSEL is contacted via a probe needle
 133 controlled by a micromanipulator. The setup further uses
 134 an optical telescope arrangement consisting of three lenses for
 135 collimating and guiding the VCSEL emission towards the mea-
 136 surement head of a Newport 1830-C powermeter. In order to
 137 determine the Stokes parameters, the methode of the rotating
 138 quarter wave-plate is applied [18, 26, 27]. For this purpose a
 139 quarter wave-plate on an automatized rotation mount and a
 140 linear polarizer are inserted into the optical path in front of the
 141 powermeter head. A mechanical stop is used to ensure a fixed
 142 orientation of the VCSEL chip for all measurements. While the
 143 polarizer is kept fixed, the quarter wave-plate is rotated and
 144 the intensity on the powermeter head detected. The intensity
 145 detected on the powermeter head in dependence of the quarter
 146 wave-plate rotation angle θ follows

$$I = \frac{1}{2} (A + B \sin(2\theta) + C \cos(4\theta) + D \sin(4\theta)), \quad (4)$$

147 where the Stokes parameters S_0, S_1, S_2 and S_3 are obtained from
 148 according to

$$S_0 = A - C, \quad S_1 = 2C, \quad S_2 = 2D, \quad S_3 = B. \quad (5)$$

149 **Results and discussion.** The structure reported in Fig. 2 is
 150 simulated by means of our DD model. Its band diagram under
 151 an applied bias voltage of 3 V is reported in Fig. 3. We sketch
 152 with different colors the longitudinal extension of the cap layer,
 153 the p-DBR, the cavity, the n-DBR and the substrate, from left to
 154 right. The electrostatic field distribution is characterize by strong
 155 peaks at the hetero-interfaces of the DBR (mitigated in the top
 156 p-DBR by the compositional grading) and is independent from
 157 the applied voltage. This profile induces an EOE anisotropy
 158 that depends solely on the aluminum molar fraction and dop-
 159 ing profiles. As a result, the emitted polarization is unaffected

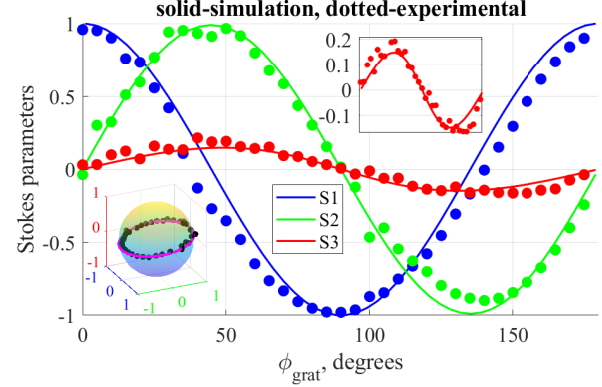


Fig. 5. Stokes parameters as function of ϕ_{grat} , both simulated (solid) and experimental (dotted). Insets represent the Stokes parameters on the Poincaré sphere (bottom left) and a zoom of S_3 (top right).

160 by the DC bias point. At this stage, optical simulations can be
 161 carried out. Before incorporating the grating effects, we focus
 162 exclusively on the EOE using Eq. (2). The resulting SW can be
 163 superimposed with the anisotropy profile, $\Delta\epsilon_{\text{EOE}}$, as shown in
 164 Fig. 4. This analysis is important for understanding the signifi-
 165 cant impact of the EOE on device performance. Despite the null
 166 average of $E(z)$, the positive peaks within the DBRs are aligned
 167 with the nodes of the SW and, consequently, minimally interact
 168 with the optical mode. Conversely, negative peaks coincide with
 169 the antinodes of the SW, resulting in an averaged anisotropy
 170 calculated as:

$$\langle \Delta\epsilon_{\text{EOE}} \rangle = \frac{\int dz \Delta\epsilon_{\text{EOE}}(z) \cdot \text{SW}(z)}{\int dz \text{SW}(z)}, \quad (6)$$

171 amounting for this structure to -3.55×10^{-4} .

172 This anisotropy is aligned with the crystal axes defined in
 173 Fig. 2 and can interact with the misaligned anisotropy of the
 174 grating, effectively forming a 3D chiral cavity that induces el-
 175 liptical polarization [16]. This phenomenon is confirmed by
 176 analyzing the calculated output Stokes parameters of the las-
 177 ing polarization, see Eq. (1d), and comparing them with mea-
 178 surements obtained for varying tilting angles ϕ_{grat} , as shown in Fig. 5.
 179 When $\phi_{\text{grat}} = 0^\circ, 90^\circ, 180^\circ$, $S_3 = 0$ so the polarization is purely
 180 linear, as all anisotropies are aligned with crystal axes, while for
 181 intermediate angles polarization is elliptical.

182 The excellent agreement between computed and experimen-
 183 tal Stokes parameters proves that VCSELs with SWG tilted to

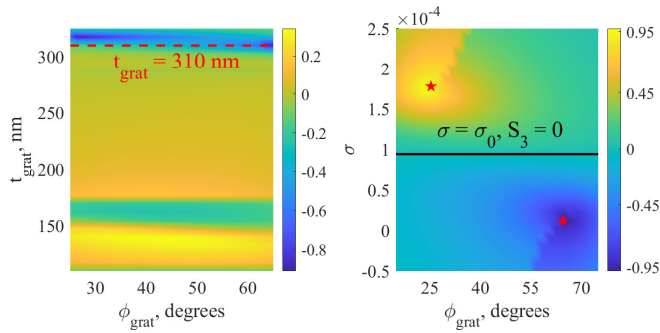


Fig. 6. Left: S_3 component of the lasing output polarization varying t_{grat} and ϕ_{grat} , the red dashed line associated to the grating thickness for which S_3 is largest in magnitude. Right: S_3 component of the output polarization varying σ and ϕ_{grat} keeping $t_{\text{grat}} = 310$ nm, the black solid line is associated to σ_0 and linear output polarization.

the crystal axes can emit elliptical polarization without modifying the state-of-the-art manufacturing processes. When strain is applied, the averaged anisotropy in Eq. (6) is modified and it is possible to obtain a linear dependence as:

$$\begin{aligned} \langle \Delta \epsilon \rangle &= \frac{\int dz (\Delta \epsilon_{\text{EOE}}(z) + \Delta \epsilon_{\sigma}(z)) \cdot SW(z)}{\int dz SW(z)} = \\ &= \langle \Delta \epsilon_{\text{EOE}} \rangle + \sigma \left(\frac{p_{44}}{2} \frac{\int dz n_r^4(z) SW(z)}{\int dz SW(z)} \right). \end{aligned} \quad (7)$$

For the device under study, it holds $\langle \Delta \epsilon \rangle = -3.55 \times 10^{-4} + 3.77\sigma$. This formula implies that the overall averaged intrinsic anisotropy can be zero when an external strain $\sigma_0 = 9.4 \times 10^{-5}$ is applied, thus eliminating the competition between the tilted grating anisotropy and the intrinsic ones. In this special case, the output polarization is always linear and oriented according to ϕ_{grat} .

Our model, as proved by the excellent comparison with the experimental results, allows to understand how lasing polarization depends on geometrical parameters such as ϕ_{grat} , t_{grat} and mechanically applied strain σ [28]. A simulation campaign is reported in Fig. 6. On the left map the Stokes parameter S_3 is reported as a function of ϕ_{grat} and t_{grat} , reaching a large negative value for $t_{\text{grat}} \simeq 310$ nm. Fixing this value, the right map displays the behavior of S_3 for varying ϕ_{grat} and σ , showing how a complete custom polarization control is possible in real-world standard grating VCSELs, including $S_3 = \pm 1$ at the red stars. As expected from Eq. (7), $\sigma = \sigma_0$ implies $S_3 = 0$, allowing for linear polarization control oriented along the grating angle, suitable for quantum key distribution applications [29].

Conclusions. In this work, we theoretically and experimentally demonstrated how the interaction between tilted optical anisotropies enable VCSELs custom polarization states. Our results highlight the value of fast and efficient simulation campaigns in understanding how polarization depends on geometric and technological parameters, paving the way for the design of CP VCSELs. A key advantage of this approach over other meta-structured chiral layers is its reliance on well-established grating VCSEL technology, ensuring compatibility with existing fabrication processes.

Acknowledgment. We appreciate the discussion within the Center of Excellence (CoE) VCSELence Turin. This work was supported by NRRP

Grant PE00000001 Program RESTART, Project RIGOLETTO. Part of the project is funded by the German Federal Ministry for Economical Affairs and Climate Action via the projects i-FPS Phase 2 (FKZ. 50YH2204B) and i-FPS Phase 2a (FKZ. 50YH2404C). We thank S. Vollmer for technical support with the MOVPE.

Disclosures. The authors declare no conflicts of interest.

Data Availability Statement. Data underlying the results presented in this paper are not publicly available at this time but may be obtained from the authors upon reasonable request.

REFERENCES

- H.-T. Cheng, Y.-C. Yang, T.-H. Liu, and C.-H. Wu, *Photonics* **9** (2022).
- M. D'Alessandro, V. Torrelli, F. Bertazzi, *et al.*, *IEEE Photonics J.* **16**, 1 (2024).
- M. Dummer, K. Johnson, S. Rothwell, *et al.*, "The role of VCSELs in 3D sensing and LiDAR," in *Optical Interconnects XXI*, vol. 11692 H. Schröder and R. T. Chen, eds., International Society for Optics and Photonics (SPIE, 2021), p. 116920C.
- G. Pan, M. Xun, X. Zhou, *et al.*, *Light. Sci. & Appl.* **13**, 229 (2024).
- N. A. Maleev, S. A. Blokhin, M. A. Bobrov, *et al.*, *Gyroscopy Navig.* **9**, 177 (2018).
- Y. Zhou, Y. Jia, X. Zhang, *et al.*, *Opt. Express* **30**, 8991 (2022).
- L. S. Watkins, C. Ghosh, J.-F. Seurin, *et al.*, *Proc. SPIE* 9616 p. 96160J (2015).
- K. Jin, X. Geng, Z. Liang, *et al.*, *MDPI Electron.* **11**, 3666 (2022).
- J. Kitching, *Appl. Phys. Rev.* **5** (2018).
- D. Liang, C. Zhang, P. Zhang, *et al.*, *nature communications* **15**, 7660 (2024).
- V. Torrelli, A. Gullino, A. Tibaldi, *et al.*, *IEEE Photonics J.* **16**, 1 (2024).
- P. Debernardi and G. P. Bava, *IEEE J. Sel. Top. Quantum Electron.* **9**, 905 (2003).
- J. M. Ostermann, P. Debernardi, C. Jalics, *et al.*, *Vertical-Cavity Surface-Emitting Lasers VIII*, *Proc. SPIE* 5364 (2004).
- P. Debernardi, J. Ostermann, M. Feneberg, *et al.*, *IEEE J. Sel. Top. Quantum Electron.* **11**, 107–116 (2005).
- P. Debernardi, J. M. Ostermann, M. Sondermann, *et al.*, *IEEE J. Sel. Top. Quantum Electron.* **13**, 1340 (2007).
- V. Torrelli, M. D'Alessandro, W. Elsässer, and P. Debernardi, *Opt. Lett.* **49**, 3773 (2024).
- G. G. Stokes, *Trans. Camb. Philos. Soc.* **9**, 399 (1852). Reprinted in *Mathematical and Physical Papers* by Cambridge University Press (2009).
- A. Molitor, S. Hartmann, and W. Elsässer, *Opt. Lett.* **37**, 4799 (2012).
- M. G. Moharam and T. K. Gaylord, *J. Opt. Soc. Am.* **71**, 811 (1981).
- L. Li, *J. Opt. Soc. Am. A* **13**, 1870 (1996).
- P. Debernardi and G. P. Bava, *Phys. Status Solidi A* **188**, 967 (2001).
- G. Sinatkas, T. Christopoulos, O. Tsilipakos, and E. E. Kriezis, *J. Appl. Phys.* **130**, 010901 (2021).
- S. Adachi, ed., *Properties of Aluminium Gallium Arsenide*, EMIS Datareviews Series (INSPEC, London, 1993).
- A. Tibaldi, F. Bertazzi, M. Goano, *et al.*, *IEEE J. Sel. Top. Quantum Electron.* **25**, 1500212 (2019).
- A. Gullino, A. Tibaldi, F. Bertazzi, *et al.*, *MDPI Appl. Sci.* **11**, 6908 (2021).
- B. Schaefer, E. Collett, R. Smyth, *et al.*, *Am. J. Phys.* **75**, 163 (2007).
- A. Molitor, P. Debernardi, S. Hartmann, and W. Elsässer, *Opt. Lett.* **38**, 4777 (2013).
- T. Pusch, M. Lindemann, N. Gerhardt, *et al.*, *Electron. Lett.* **51**, 1600 (2015).
- M. Zimmer, M. Birkhold, M. Jetter, and P. Michler, "Monolithic 850 nm VCSEL array for quantum key distribution via the BB84 and decoy state protocol," in *Vertical-Cavity Surface-Emitting Lasers XXVIII*, vol. PC12904 C. Lei and K. D. Choquette, eds., International Society for Optics and Photonics (SPIE, 2024), p. PC1290402.

FULL REFERENCES

- 283
284
285
286
287
288
289
290
291
292
293
294
295
296
297
298
299
300
301
302
303
304
305
306
307
308
309
310
311
312
313
314
315
316
317
318
319
320
321
322
323
324
325
326
327
328
329
330
331
332
333
334
335
336
337
338
339
340
341
342
343
344
345
346
347
348
349
350
1. H.-T. Cheng, Y.-C. Yang, T.-H. Liu, and C.-H. Wu, "Recent advances in 850 nm vcsels for high-speed interconnects," *Photonics* **9** (2022).
2. M. D'Alessandro, V. Torrelli, F. Bertazzi, *et al.*, "Transverse coupled cavity vcsels: Bridging ultrabroadband dynamics to optical supermodes," *IEEE Photonics J.* **16**, 1–7 (2024).
3. M. Dummer, K. Johnson, S. Rothwell, *et al.*, "The role of VCSELS in 3D sensing and LiDAR," in *Optical Interconnects XXI*, vol. 11692 H. Schröder and R. T. Chen, eds., International Society for Optics and Photonics (SPIE, 2021), p. 116920C.
4. G. Pan, M. Xun, X. Zhou, *et al.*, "Harnessing the capabilities of vcsels: unlocking the potential for advanced integrated photonic devices and systems," *Light. Sci. & Appl.* **13**, 229 (2024).
5. N. A. Maleev, S. A. Blokhin, M. A. Bobrov, *et al.*, "Laser source for a compact nuclear magnetic resonance gyroscope," *Gyroscopy Navig.* **9**, 177–182 (2018).
6. Y. Zhou, Y. Jia, X. Zhang, *et al.*, "Large-aperture single-mode 795 nm VCSEL for chip-scale nuclear magnetic resonance gyroscope with an output power of 4.1 mW at 80°C," *Opt. Express* **30**, 8991–8999 (2022).
7. L. S. Watkins, C. Ghosh, J.-F. Seurin, *et al.*, "High power VCSEL devices for atomic clock applications," *Proc. SPIE* 9616 p. 96160J (2015).
8. K. Jin, X. Geng, Z. Liang, *et al.*, "Design of portable self-oscillating VCSEL-pumped cesium atomic magnetometer," *MDPI Electron.* **11**, 3666 (2022).
9. J. Kitching, "Chip-scale atomic devices," *Appl. Phys. Rev.* **5** (2018).
10. D. Liang, C. Zhang, P. Zhang, *et al.*, "Evolution of laser technology for automotive lidar, an industrial viewpoint," *nature communications* **15**, 7660 (2024).
11. V. Torrelli, A. Gullino, A. Tibaldi, *et al.*, "High-power emission via large-area vcsels with single high-order mode operation," *IEEE Photonics J.* **16**, 1–7 (2024).
12. P. Debernardi and G. P. Bava, "Coupled mode theory: a powerful tool for analyzing complex VCSELS and designing advanced devices features," *IEEE J. Sel. Top. Quantum Electron.* **9**, 905–917 (2003).
13. J. M. Ostermann, P. Debernardi, C. Jalics, *et al.*, "Monolithic polarization control of multimode VCSELS by a dielectric surface grating," *Vertical-Cavity Surface-Emitting Lasers VIII*, Proc. SPIE 5364 (2004).
14. P. Debernardi, J. Ostermann, M. Feneberg, *et al.*, "Reliable polarization control of VCSELS through monolithically integrated surface gratings: a comparative theoretical and experimental study," *IEEE J. Sel. Top. Quantum Electron.* **11**, 107–116 (2005).
15. P. Debernardi, J. M. Ostermann, M. Sondermann, *et al.*, "Theoretical-experimental study of the vectorial modal properties of polarization-stable multimode grating vcsels," *IEEE J. Sel. Top. Quantum Electron.* **13**, 1340–1348 (2007).
16. V. Torrelli, M. D'Alessandro, W. Elsässer, and P. Debernardi, "On-demand polarization by a vertical-cavity surface-emitting laser with two tilted sub-wavelength gratings," *Opt. Lett.* **49**, 3773–3776 (2024).
17. G. G. Stokes, "On the composition and resolution of streams of polarized light from different sources," *Trans. Camb. Philos. Soc.* **9**, 399–416 (1852). Reprinted in *Mathematical and Physical Papers* by Cambridge University Press (2009).
18. A. Molitor, S. Hartmann, and W. Elsässer, "Stokes vector characterization of the polarization behavior of vertical-cavity surface-emitting lasers," *Opt. Lett.* **37**, 4799 (2012).
19. M. G. Moharam and T. K. Gaylord, "Rigorous coupled-wave analysis of planar-grating diffraction," *J. Opt. Soc. Am.* **71**, 811 (1981).
20. L. Li, "Use of fourier series in the analysis of discontinuous periodic structures," *J. Opt. Soc. Am. A* **13**, 1870 (1996).
21. P. Debernardi and G. P. Bava, "Effects of anisotropies on vectorial modes of vertical-cavity surface-emitting lasers," *Phys. Status Solidi A* **188**, 967–977 (2001).
22. G. Sinatkas, T. Christopoulos, O. Tsilipakos, and E. E. Kriezis, "Electro-optic modulation in integrated photonics," *J. Appl. Phys.* **130**, 010901 (2021).
23. S. Adachi, ed., *Properties of Aluminium Gallium Arsenide*, EMIS Datareviews Series (INSPEC, London, 1993).
24. A. Tibaldi, F. Bertazzi, M. Goano, *et al.*, "VENUS: a Vertical-cavity surface-emitting laser Electro-opto-thermal NUMerical Simulator," *IEEE J. Sel. Top. Quantum Electron.* **25**, 1500212 (2019).
25. A. Gullino, A. Tibaldi, F. Bertazzi, *et al.*, "Reduced dimensionality multiphysics model for efficient VCSEL optimization," *MDPI Appl. Sci.* **11**, 6908 (2021).
26. B. Schaefer, E. Collett, R. Smyth, *et al.*, "Measuring the stokes polarization parameters," *Am. J. Phys.* **75**, 163–168 (2007).
27. A. Molitor, P. Debernardi, S. Hartmann, and W. Elsässer, "Spatially resolved stokes parameters of small-area vertical-cavity surface-emitting lasers: experiment and simulation," *Opt. Lett.* **38**, 4777–4780 (2013).
28. T. Pusch, M. Lindemann, N. Gerhardt, *et al.*, "Impact of in-plane anisotropic strain on the polarization behavior of vertical-cavity surface-emitting lasers," *Electron. Lett.* **51**, 1600–1602 (2015).
29. M. Zimmer, M. Birkhold, M. Jetter, and P. Michler, "Monolithic 850 nm VCSEL array for quantum key distribution via the BB84 and decoy state protocol," in *Vertical-Cavity Surface-Emitting Lasers XXVIII*, vol. PC12904 C. Lei and K. D. Choquette, eds., International Society for Optics and Photonics (SPIE, 2024), p. PC1290402.